Effect of Shot Peening Treatment on Residual Stress and Magnetic Barkhausen Noise of AISI 201LN and AISI 304L Stainless Steels

Marcel Freitas de Souza[a] (ID)*, Juan Manuel Pardal[a], Hugo Ribeiro da Igreja[a],*

*Linilson Rodrigues Padovese[b], Maria Cindra Fonseca[a]** (ID)

[a]*Universidade Federal Fluminense, Departamento de Engenharia Mecânica, Pós-Graduação em Engenharia Mecânica (PGMEC), Escola de Engenharia, Niterói, RJ, Brasil.*
[b]*Universidade de São Paulo, Departamento de Engenharia Mecânica, Escola Politécnica, São Paulo, SP, Brasil.*

This work evaluates microstructural changes and residual stresses on surface samples of AISI 201LN and 304L subjected to shot peening. The residual stresses were measured by Xray diffraction and magnetic Barkhausen noise (MBN) in different shot-peened conditions. The results showed that the 201LN steel presented more martensite than the 304L steel in the initial condition, but with lower δferrite contents. These ferromagnetic phases were present in a low amount with high tensile residual stresses due to brush cleaning and light coldrolling in the final stage of the fabrication process. The shot peening process promoted compressive residual stresses mainly in the δferrite. However, some "fresh" martensite exhibited tensile residual stress represented by higher and thinner peaks, which together with the low-intensity amplitude in the neighborhood, represented all formed martensite. Thus, small microstructural changes provoked high residual stresses behavior, which can be detected in ferromagnetic phases by MBN.

Keywords: *201LN steel, 304L steel, Residual stress, X-ray diffraction, Barkhausen noise.*

1. Introduction

Austenitic stainless steels (ASS) have good mechanical properties and corrosion resistance, and for this reason are used in various industrial sectors, such as equipment for food, pharmaceutical, nuclear, aerospace and petroleum industries[1,2]. In this family of austenitic stainless steels, the 300 series is the most commonly used and is characterized by a high content of chromium and nickel. However, due to nickel price volatility in the international market, other austenite stabilizer elements, such as nitrogen and manganese, can replace this metal, giving rise to the 200 series. Therefore, new stainless steels, such as 201LN steel, characterized by low carbon content and nitrogen addition, are being investigated to achieve lower cost production[3,4].

Nevertheless, in some stainless steel designations, the austenite phase is more metastable and promotes austenite transformation into martensite, achieving the desired mechanical properties, mainly due to the chemical composition. In this way, stacking fault energy (SFE) plays a major role in martensitic transformation, but grain size, degree of deformation and temperature also contribute to this mechanism[5].

SFE determines the main hardening mechanism associated with plastic deformation of austenitic stainless steel. The decrease in SFE causes slip dislocations and allows mechanical twins or the formation of martensite by deformation. A stacking fault energy greater than 20 mJ/m² inhibits paramagnetic εmartensite formation and enables the α'martensite formation reaction (γ→ twin→ α'). In contrast, the γ→ε→α' reaction is observed at low SFE. In this case, in the initial deformation stage, shear bands with stacking fault and twins are generated in the γ-phase, leading to the ε-martensite formation by stacking faults overlapping and α'-phase nucleated at the intersection of ε-martensite bands and in regions close to the bands[6].

The 200 series has lower SFE than the 300 series and is more prone to the γ→ε→α' reaction. This metallurgical transformation alters not only the residual stresses but also the magnetic properties of the material, since the gamma iron crystalline structure is paramagnetic, while the α'martensite, with a body-centered cubic structure, is ferromagnetic[7,8].

Mechanical treatments, such as shot peening, are used in the manufacturing process to produce a compressive residual stresses state on the surface material, improving the component fatigue service life, since the nucleation and propagation of fatigue cracks are mitigated by these compressive residual stresses. Therefore, it is essential to analyze the shot peening time effect on microstructural change and residual stresses state, taking into account results obtained in ASS's by shot peening treatment[9] and cold-rolling process[10], where both studies highlighted a martensitic transformation with more tensile behavior in the early phase of plastic deformation. However, it is important to evaluate the initial influence in

this process of delta ferrite amount, which depends on the chromium and nickel equivalent ratio and the plate thickness[11].

X-ray and neutron diffraction are standard nondestructive methods for assessing the residual stresses generated by the shot peening process. X-ray diffraction is more cost-effective for the analysis of shot-peened surface[12], but special care must be taken when performing it in the field, such as logistics, accessibility, isolation and professionals with extreme qualifications.

Although MBN is an experimental technique, it has significant potential for industrial applications. This technique is sensitive to many features, such as microstructural phase change and precipitation, hardness and residual stresses. The consolidation of this method, especially for shot-peened materials, requires complementary analysis by hardness test, metallography and another technique, such as X-ray diffraction, to understand the material behavior[13,14].

In this context, this work studies the residual stresses obtained by X-ray diffraction technique, applying the $\sin^2\psi$ method, and MBN in ASS 201LN and 304L subjected to shot peening up to 90 seconds. Ferritoscopy and surface hardness measurements complement this study.

2. Materials and Methods

The ASS 201LN and 304L were manufactured according to ASTM A240[15] and supplied in the form of 6 mm and 10 mm thick plates, respectively. The chemical compositions of the two materials are listed in Table 1.

The stacking fault energy (SFE) was calculated according to the methodology proposed by Curtze et al.[16] using a program developed in another work of our group[5].

The chromium and nickel equivalents were estimated using Equation 1 and Equation 2, respectively[17,18].

$$Cr_{eq}\left(wt.\%\right) = Cr + 2Si + 1.5Mo + 5V + 5.5Al + 1.75Nb + 1.5Ti + 0.75W \quad (1)$$

$$Ni_{eq}\left(wt.\%\right) = Ni + Co + 0.5Mn + 0.3Cu + 25N + 30C \quad (2)$$

The increase in chromium and nickel equivalent ratio and the greater plate thickness indicate a higher susceptibility of amounts in the microstructure of delta ferrite, with the approximate ratio of 1.48 representing the transition in solidification behavior from primary austenite to primary ferrite[19,20].

Analysis by light optical microscopy (LOM) was performed on the as-received surface, revealed by electrolytic aqueous etching with 10% of oxalic acid ($C_2H_2O_4$) for 90 seconds. The delta ferrite observed in metallography was quantified according to ASTM E112[21] for both materials.

The X-ray diffraction analysis for phase characterization in the as-received condition was performed on a Bruker D8 Advance diffractometer, using CuKα radiation with wavelength λ = 1.544 Å and monochromator. The tests used a 2θ scanning angle range of 1095°. The measurements were performed at room temperature in continuous scanning mode, with an angular step of 0.02° and a counting time of 0.2 second. The voltage and current used were 40 kV and 40 mA, respectively. The phase quantification was performed by the Rietveld method employing X'pert HighScore software[22].

Tensile tests of ASS 201LN and 304L in as-received conditions were carried out at room temperature using a 250 kN Instron mechanical testing machine at 5 mm/min. Three tensile specimens of each material were machined in the longitudinal rolling direction (RD) according to the dimensions specified in ASTM A370[23].

Three samples of each material were prepared by machining with the length parallel to the rolling direction and dimensions of 76.20 x 19.05 mm[24]. Then, the machined specimens were subjected to manual shot peening at room temperature using glass microspheres with a diameter of 152250 μm and working pressure of 550 MPa, considering a distance of 50 mm perpendicular to the surface. The samples were submitted to 30, 60 and 90-second treatments to evaluate changes in microstructural, hardness and residual stresses. It is important to highlight that in each 15-second treatment, the surface was completely (100%) covered by the treatment.

Twenty measurements were made for each sample condition to quantify the ferromagnetic phases, using a ferritoscope Helmut Fischer model FMP 30. The correction of 1.7 was applied to evaluate the martensite content[25].

Twenty measurements of surface hardness Rockwell test, according to ASTM E18[26], were made for each condition using a 1/16" steel ball penetrator with 3 kg preload and 15 kg load (HR 15T). The Rockwell hardness test (scale T) is a Rockwell superficial hardness test similar to Rockwell hardness test except that smaller preliminary and total test forces are used with a shorter depth scale and, consequently, the volume of metal deformed by the indenter is significantly reduced[26]. Analysis of variance (ANOVA) test was used to confirm the effect of shot peening time on the quantification of ferromagnetic phases and surface hardness.

Residual stresses were analyzed by X-ray diffraction technique using $\sin^2\psi$ method and performed with Xstress 3000 analyzer with a collimator of ∅ 2.0 mm (30 kV and 6.7 mA). The XTronic V10 Standard software was used to perform the stress calculation. The parameters are given in Table 2.

Table 1. Chemical composition (wt.%) of ASS 201LN and 304L (Fe in balance).

	C	Mn	Si	P	S	Cr	Ni	Mo
201LN	0.0237	7.0178	0.3823	0.0372	0.0014	17.0586	4.0698	0.0429
	Al	**Cu**	**Co**	**V**	**Nb**	**Ti**	**W**	**N**
	0.0047	0.0717	0.0616	0.0408	0.0038	0.0041	0.0147	0.1640
304L	**C**	**Mn**	**Si**	**P**	**S**	**Cr**	**Ni**	**Mo**
	0.0204	1.3157	0.4536	0.0331	0.0015	18.0608	8.0119	0.1113
	Al	**Cu**	**Co**	**V**	**Nb**	**Ti**	**W**	**N**
	0.0032	0.216	0.1824	0.0509	0.0072	0.0023	0.0236	0.0501

Effect of Shot Peening Treatment on Residual Stress and Magnetic Barkhausen Noise of AISI 201LN and AISI 304L Stainless Steels

3

The residual stresses in austenite and ferrite plus martensite were evaluated on the surface center in the longitudinal rolling direction in each sample before and after shot peening.

The MBN measurements were carried out to evaluate the root mean square (RMS) level over time, comparing the signal obtained between shot-peened conditions and asreceived samples. This test used a probe of 80 mm² cross-section yoke of Fe-Si grainoriented core in which a 22 American Wire Gauge (AWG) primary excitation coil was wound with 200 turns around the center core with 1 Ω electrical impedance. The secondary coil for analyzing the MBN comprises 44 AWG wire wound on one end of the core with 2000 turns and 330 Ω electrical impedance. The test was conducted by applying of 3.5 V with a sinusoidal excitation frequency of 50 Hz. The signal was obtained with a sampling frequency of 350 kHz, applying a 150 kHz as anti-aliasing filter and band-pass filter between 12 and 60 kHz.

The depth penetration of MBN signal is damped due to the skin effect, which is caused by the opposing eddy currents induced by the changing magnetic field. The damping of a noiselike signal as a Barkhausen noise, containing a spectral distribution of frequencies between f_1 and f_2, can be described by a function of $D(x)$ as described in Equation 3, where $g(f)$ is the frequency spectrum of the captured signal within the selected frequency range, x is the depth of detection, $A = \sqrt{\pi \mu / \rho}$, μ is the permeability of the material and ρ is the electrical resistivity of the material[27,28].

$$D(x) = \frac{\int_{f_2}^{f_1} g(f) \cdot e^{-Ax\sqrt{f}} \, df}{\int_{f_2}^{f_1} g(f) \, df} \tag{3}$$

Analysis performed near the resonance frequency of the sensor provides greater sensitivity, because noise of greater amplitude is generated in this frequency range[29]. However, when working outside the sensor resonance frequency, a sharp decrease in sensitivity is observed. This phenomenon was taken into account in this work by simplifications adopted from the spectrum density profile to analyze analytically the behavior of the signal response. Thus, small intervals of 5 kHz between 70 and 85 kHz were considered for the analysis. In addition, another methodology was considered in accordance with Zerovnik and Grum[30], where bandpass filters were applied in the proposed interval range between 70 and 85 kHz. In this way, a constant function $g(f)$ for each proposed interval agrees with the effects of the nonlinear profile of this spectral range. The attenuation

signal associated with the detection depth considers 37% of the detected $D(x)$ (or $1/e$)[30].

Finally, Figure 1 shows all tests performed in these materials.

3. Results and Discussion

Figure 2 shows the microstructure obtained by light optical microscopy (LOM), where austenitic grains with twins without eventually any martensite traces are observed. In the micrograph, the dark phase indicated by white arrows represents the elongated delta ferrite, which was verified in the rolling direction (RD)[31,32]. Because of the greater Cr_{eq}/Ni_{eq} ratio and plate thickness, the ASS 304L was more susceptible to have delta ferrite than the ASS 201LN.

According to ASTM E112[21], the average grain size determined through the intercept method using ImageJ[33] was 18±4 μm for 201LN steel and 25±5 μm for 304L steel.

Figure 3 shows the diffractogram of 201LN and 304L steels in the as-received state. In these conditions, there were distinguishable α'-martensite and/or δ-ferrite in (110) and a small peak in (101) planes of ε-martensite relative to the 201LN. This feature was attributed to the greater metastability of 201LN associated with lower a SFE value than 304L when applying the methodology proposed by Curtze et al.[16].

Table 3 shows the plate thickness, Cr_{eq}/Ni_{eq} ratio and SFE values to corroborate the amounts of delta ferrite plus martensite measured by LOM, X-ray diffraction and ferritoscope techniques for ASS 201LN and 304L in the as-received condition. In this way, the amount of delta ferrite quantified by LOM on the surface was greater in the 304L than 201LN. In contrast, the X-ray diffraction only distinguished delta ferrite plus martensite close to the surface of 201LN steel.

Finally, ferritoscope measurement evaluated these ferromagnetic phases in depths around 1 mm[34]. The ferritoscope considered the presence of martensite in superficial layers
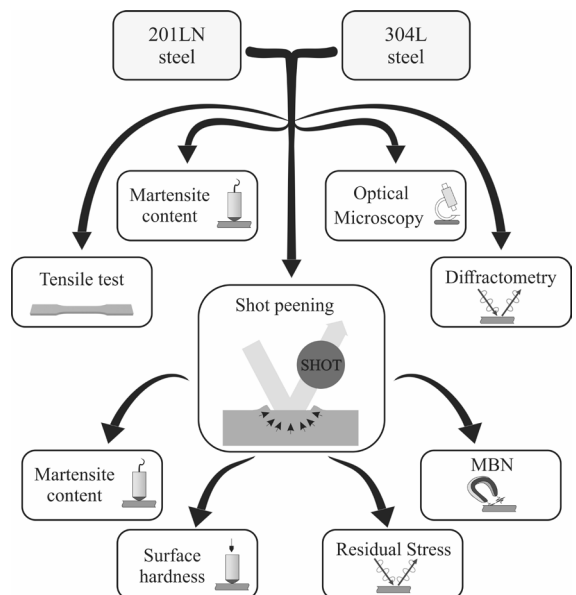
Table 2. Parameters used for the X-ray residual stresses analysis.

	Austenite	Ferrite + Martensite
Diffraction plane (hkl)	(311)	(211)
Diffraction angle 2θ (°)	148.52	156.41
Radiation	CrKβ	CrKα
Inclination angle ψ (°)	0, 18, 27, 33, 45	0, 18, 27, 33, 45
Exposure time (s)	20	5

Figure 1. Flow chart describing the performed tests.

Table 3. Influencing parameters and phase quantification of delta ferrite and martensite.

Types	Influencing parameters of Ferrite + Martensite			Ferrite content (%)	Ferrite + Martensite content (%)	
	Thickness (mm)	Cr_{eq}/Ni_{eq}	SFE (mJ/m²)	LOM	X-ray diffraction	Ferritscopy
201LN	6	1.45	21.30	1.2±0.4	3.9	1.57±0.11
304L	10	1.80	27.39	2.6±0.6	0	0.96±0.06
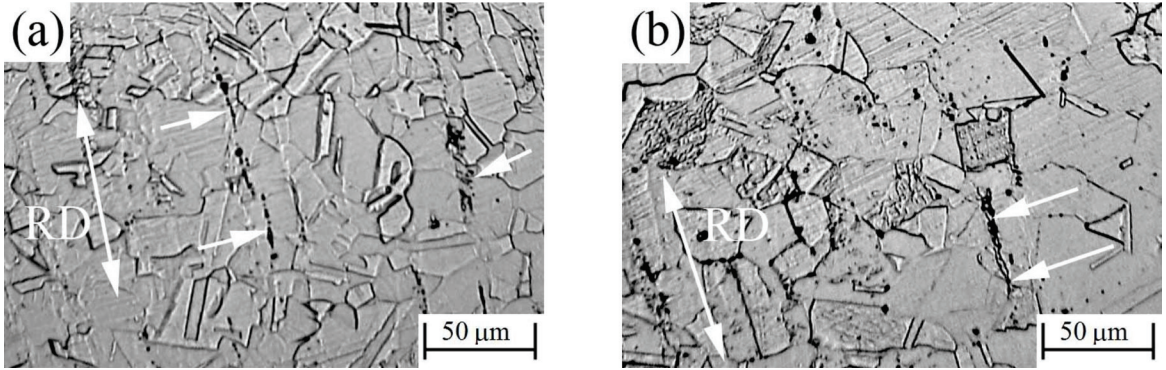
Figure 2. Microstructure in the as-received condition of ASS: (a) 201LN and (b) 304L.
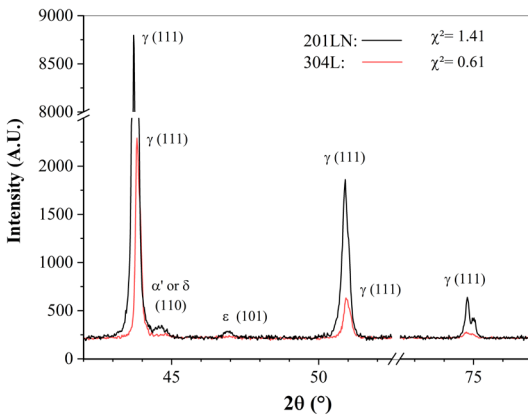
Figure 3. Diffractogram for 201LN and 304L steels in the as-received condition. Lower goodnessoffit (χ^2) values were obtained by Rietveld method fitting in both cases.

preponderantly in 201LN steel, as a consequence of brushing and coldrolling processes performed by the manufacturer.

The quantification of delta ferrite (δ) plus martensite (α') measured by ferritoscopy is shown in Figure 4a and the surface hardness Rockwell (HR 15T) is shown in Figure 4b.

The shot peening promoted a slight increase in ferromagnetic phases, measured by ferritoscopy, as an exclusive consequence of the transformation of austenite into martensite, being possible to observe a continuous increase in the evaluated range.

The standard deviation in Figure 4a after shot peening was greater than in the initial condition. The overlap of indentations caused by the bombardment of the spheres on the surface promoted heterogeneity with respect to the martensite content formed by the transformation induced by deformation. The analysis of variance (ANOVA) test

indicated that the application time was statistically significant, with a p-value tending towards zero for both materials and a square mean of 44.63 for 201LN and a square mean of 33.22 for 304L.

The shot peening provided a significant hardness increase in the first 30 seconds as a result of strain hardening of the austenitic matrix for both materials. Thereafter, a slight increase was observed, which is related to martensitic precipitation on the surface, as the austenitic matrix was already strain hardened and therefore did not promote the same initial percentage increase. The ANOVA test also revealed that shot peening time was statistically significant for surface hardness, with a pvalue tending towards zero for both materials and a square mean of 48.9 for 201LN steel and a square mean of 30.9 for 304L steel.

A correlation between the martensite content (MC) and the surface hardness (HR_{15T}) is described in Equation 4 and the coefficients of this equation are shown in Table 4.

$$HR_{15T} = a - b \cdot MC^{-c} \qquad (4)$$

In Equation 4 the *a* coefficient represented the maximum predict value of the surface hardness, while the *b* and *c* coefficients affected the slope of the model curves. The increase of *b* value decreases the forecast surface hardness, especially for low martensite content. The increase of *c* coefficient increases the expected response value, which would tend to the maximum value described by the *a* coefficient and consequently reducing the effect of martensite content variation on the surface hardness.

Figure 5 shows the graphical representation between delta ferrite (δ) plus martensite (α') content and surface hardness.

The model for Equation 4 had a coefficient of determination (R^2) of 0.99, expressing an excellent fit and a very reliable model for future predictions in the martensite content range. A low delta ferrite content in the as-received condition would result in a low hardness in Figure 5, which does not correspond to the real mechanical properties of these materials.
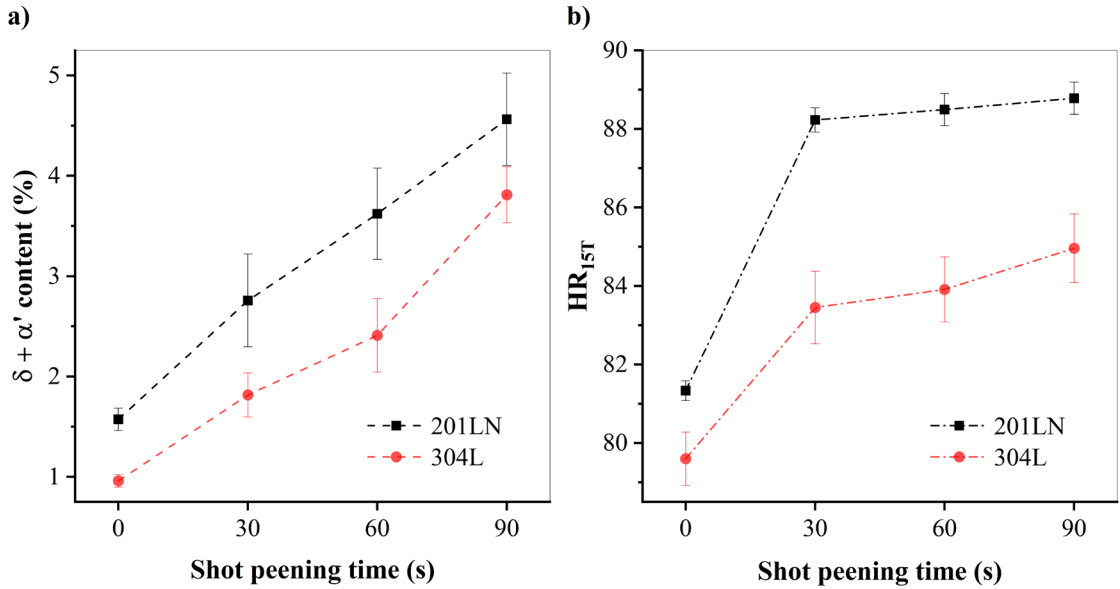
Effect of Shot Peening Treatment on Residual Stress and Magnetic Barkhausen Noise of AISI 201LN and AISI
304L Stainless Steels

5

Figure 4. (a) Phase quantification by ferritoscopy and (b) surface hardness Rockwell according to the shot peening time.
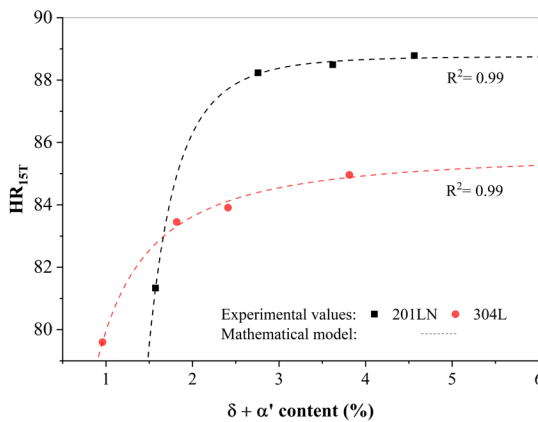

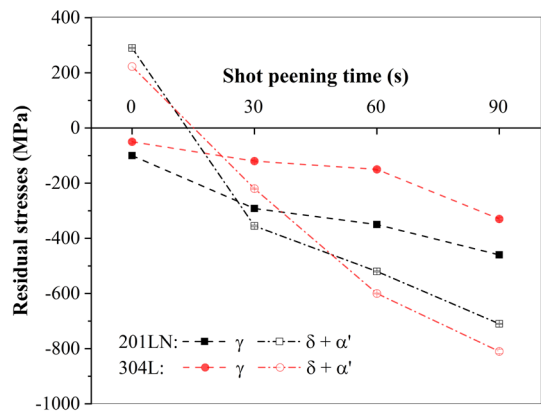**Figure 5.** Correlation between delta ferrite plus martensite content and surface hardness for 201LN and 304L steels.

Figure 6. Residual stresses in 201LN and 304L steels with different shot peening times.

Table 4. Coefficients of Equation 4 for 201LN and 304L steels.

Material	Coefficients of Equation 4			Coefficient of determination (R^2)
	a	b	c	
201LN	88.76	59.62	4.60	0.99
304L	85.66	5.70	1.48	0.99

The first part of the curves was characterized by high growth in hardness, with minimum increase of the martensite content due to the plastic deformation caused by shot peening. In the second part, after the high initial increase, both curves showed lower growth and tended to a stable level, which was explained by the martensite precipitation on the surface.

Figure 6 shows the residual stresses diffracting the austenite (γ) and delta ferrite (δ) plus martensite (α') crystallographic planes in the 201LN and 304L steels with different treatment

times. The shot peening, although introduces beneficial compressive residual stresses and improves mechanical properties, such as the fatigue resistance, also causes a surface roughness rise. Thus, as recommended by Fitzpatrick et al.[35], an electrolytic cleaning was used to assess the residual stresses in the shot-peened samples, reducing the surface roughness and improving the X-ray diffraction quality.

The residual stresses in the austenite phase were compressive in the asreceived condition with a magnitude of 100 MPa for 201LN steel and 50 MPa for 304L steel. Considering the residual stresses in delta ferrite plus martensite phase in the as-received state, both materials presented tensile values, 290 MPa for 201LN steel and 220 MPa for 304L steel.

The residual stresses in both phases were below the yield strength, whose values obtained by tensile test were 518±36 MPa and 287±9 MPa, respectively, for 201LN and 304L steels. The difference between these values was

mainly due to the higher nitrogen content of 201LN steel, since nitrogen is a strong austenite stabilizer that causes solid solution strengthening, resulting in improved strength of stainless steel. Another important effect of nitrogen is the reduction of Staking Fault Energy (SFE), as shown in Table 3, which also contributed to an increase in the mechanical properties[36,37].

The shot peening time increased the compressive residual stresses intensity in both phases and also promoted a significant inversion from tensile to compressive state for delta ferrite plus martensite phase, therefore, a minimum shot peening time was capable to produce a beneficial residual stresses state.

The behavior of residual stresses in each phase was similar for both materials. With increasing shot peening time and consequent formation of martensite by deformation, the microstructure also became more sensitive to the global characterization of residual stresses, confirming the need to study ferromagnetic phases in an austenitic matrix.

Measurements carried out in two phases are fundamental to understand the general residual stresses state, but the values are not comparable due to dissimilar deformation mechanisms and different martensite content produced with different shot peening time[35]. The measurements diffracting austenite and martensite phases had errors of the order of 10 MPa, which made the error bar negligible due to the scale adopted for the vertical axis.

Figure 7 and Figure 8 show respectively the envelope of the root mean square values of magnetic Barkhausen noise in function of the time for 201LN and 304L steels for all conditions considering the first round trip, i.e., the first peak represents the outward time and the second peak represents the return time of the signal.

In these figures, it was observed a time delay of 2 ms of the maximum RMS peak attained between the asreceived conditions in relation to the shot-peened treated samples. Therefore, shot peening brought forward the RMS peaks compared to the as-received state due to the simultaneous effect of the presence of ferromagnetic phases (i.e. delta ferrite plus martensite) and their residual stresses state. The highest RMS peaks responses were mainly related to the ferromagnetic phases with high residual stress values, while the increased background RMS values of these figures were mainly a consequence of low residual stresses values.

Thus, complex interactions were observed in the ferromagnetic phases when a small deformation was applied on the surface, because the martensite and delta ferrite from the asreceived condition became compressive. In addition, during shot peening process, a fraction of austenite was converted to martensite, called as "fresh" martensite, which presented tensile residual stresses.

Another interesting fact in the comparison of the two materials was the RMS values. ASS 201LN presented higher RMS values because of the higher metastability of the austenite due to the lower stacking fault energy (SFE) and, therefore, it was more prone to the $\gamma \rightarrow \varepsilon \rightarrow \alpha'$ reaction. In this way, this material exhibited a higher content of "fresh" martensite, which, as mentioned above, showed tensile behavior, resulting in more intense peaks compared to ASS 304L.
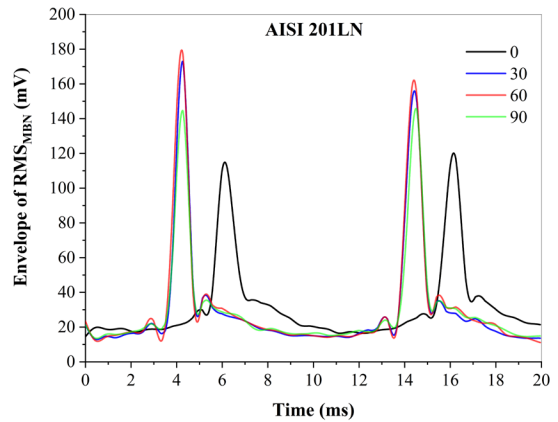

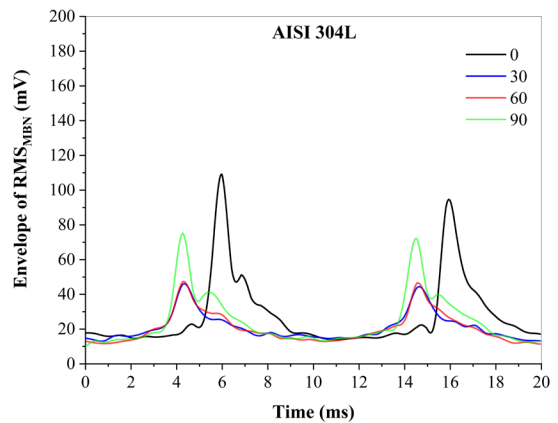**Figure 7.** Envelope of RMS$_{MBN}$ *vs.* time for 201LN steel.

Figure 8. Envelope of RMS$_{MBN}$ *vs.* time for 304L steel.

Figure 9 and Figure 10 show the frequency spectral density for 201LN and 304L steels, respectively, obtained from the RMS$_{MBN}$ values. These figures have been plotted in the same scale to distinguish comparatively the frequency domain behavior for both materials, with the largest contribution between 70 and 85 kHz, since the signal detected in this range was more sensitive, because it was close to the resonance frequency.

Although magnetic Barkhausen noise is affected by grain size, this factor can be considered less relevant in this research than the effect of microstructural and residual stresses changes. Both materials had similar grain sizes in the initial condition and the parameters used in the present shot peening treatment were of low intensity, which reduced the effect of grain refinement and, consequently, the relevance of this variable in the analysis[38].

Thus, MBN was significantly influenced by these two factors when analyzing the signal behavior in the resonance neighborhood, although, some simplifications have been taken into account when evaluating the response changes as a consequence of the presence of the ferromagnetic phase and its residual stresses state.

Taking these facts into account, Table 5 can be established, where a signal proportion analysis was estimated considering
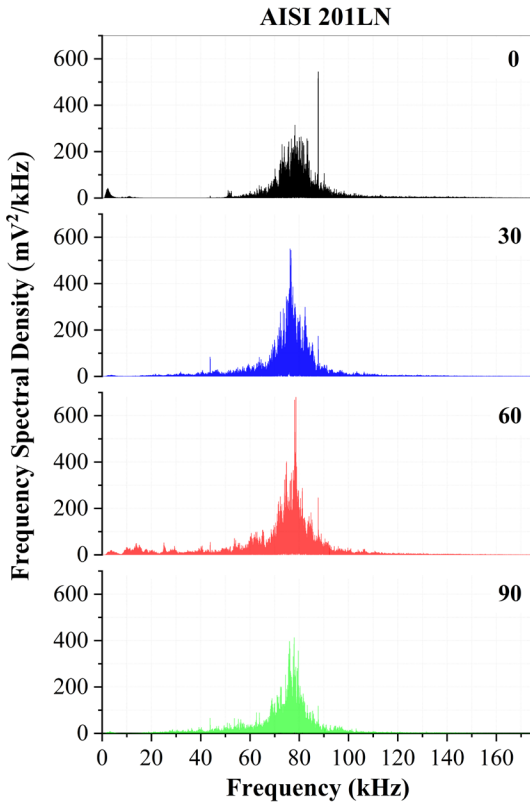
Figure 9. Frequency spectral density for 201LN steel.
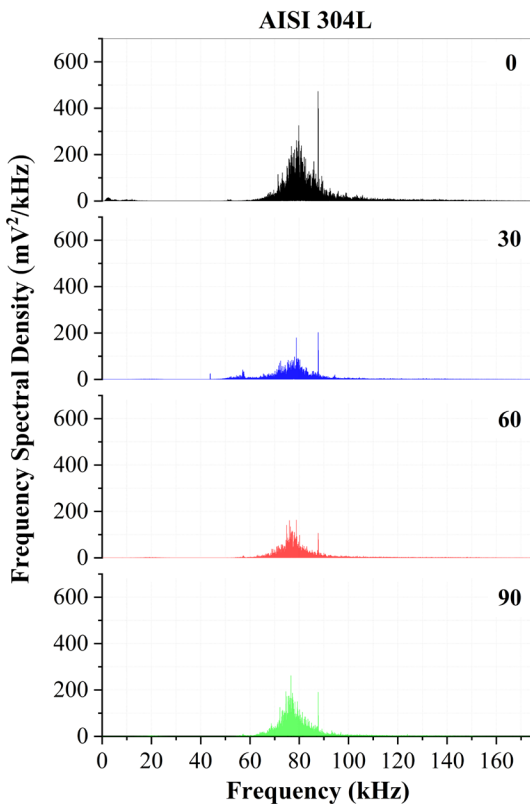

Figure 10. Frequency spectral density for 304L steel.

a small interval of 5 kHz with respect to the range between 70 and 85 kHz as a consequence of the high sensitivity of the detected MBN.

Table 5 was based on a relative comparison between the analyzed frequencies due to the resonance frequency sensitivity. In the range between 70-75 kHz, there was only a tendency for the formation of tensile "fresh" martensite only in ASS 304L shot-peened conditions in relation to the as-received state. However, between 75-80 kHz, a slight increase in the signal proportion was detected in both steels, being a product of the martensite formation with a tensile behavior. In the 80-85 kHz range, there was a decrease in the signal proportion with the treatment time, which was due to the most significant compressive residual stresses on the surface of the material.

It is worth noting that these qualitative analyzes also take into account that small changes in the microstructure occur intrinsically along the superficial layers as a product of shot peening, demonstrating that MBN is a powerful tool to analyze these phenomena[39].

This analysis by frequency range, considered comparatively, allows the evaluation of continuous damping, where there was a similar behavior in both materials, considering a permeability of 1.02 for both materials and an electrical resistivity of 68.5×10^{-8} Ω·m for 201LN steel and 72.0×10^{-8} Ω·m for 304L steel, as shown in Figure 11[40,41].

This figure considered only the initial permeability and resistivity. With the transformation of austenite into martensite, there was an increase in permeability and resistivity, and in this case, since this ferromagnetic phase precipitated only on the surface with not so high significant values, these parameters were considered very close for the analysis of the damping effect.

Another interesting fact can be observed when considering an austenitic matrix, where greater penetration depths were obtained in the signal readings compared to a microstructure with increasing martensite levels, i.e., with the formation of martensite there was an attenuation of the signal as a result of the variation of the physical parameters that interact in the formation of eddy currents. Therefore, there were differences in the evaluated depths compared to Kleber and Barroso[9].

Figures 12 and 13 present the results of the MBN signal as a function of time. The band-pass filter was used in the
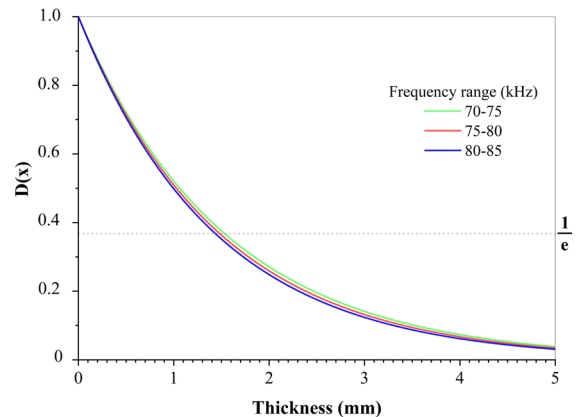

Figure 11. Damping profile for 201LN and 304L steels.

Table 5. Comparative analysis between both materials in relation to the percentage of a small frequency range in the domain near frequency resonance (70-85 kHz).

Frequency range analysis (kHz)	Frequency range proportion in relation to 70-85 kHz (%)							
	201LN (treatment time)				304L (treatment time)			
	0	30	60	90	0	30	60	90
70 – 75	26	27	32	27	17	28	25	26
75– 80	42	50	45	47	46	46	52	49
80 – 85	32	23	23	25	37	26	22	25

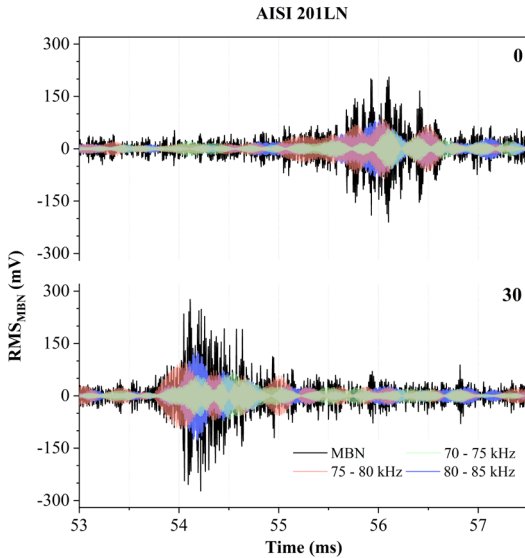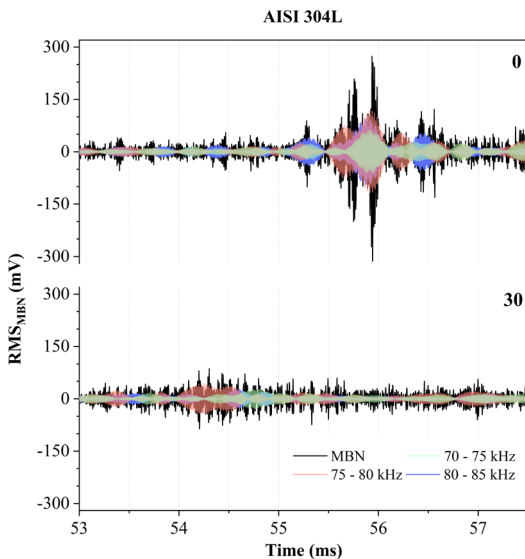**Figure 12.** RMS_{MBN} for 201LN steel.

Figure 13. RMS_{MBN} for 304L steel.

same frequency interval adopted in Table 5 to establish a comparative signal analysis in the time domain for as-received conditions and 30 seconds of shot peening treatment for the peak located between 53 and 57.5 ms.
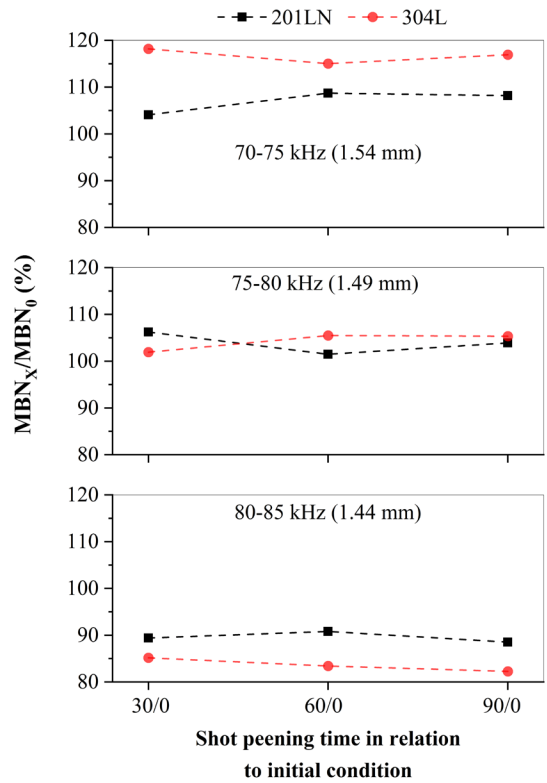

Figure 14. Proportion of RMS_{MBN} signals in relation to shot-peened conditions using bandpass filter methodology.

As expected, a significant variation in the MBN was observed for both materials in these conditions, in accordance with the preliminary results obtained by other techniques, such as Xray, LOM and ferritoscopy. However, the effect of the displacement of the mentioned signal was also associated with the considered frequency range near the resonance frequency range.

Figure 14 shows the proportional values of the RMS_{MBN} signal in relation to the initial condition when evaluating the same frequency range for both materials as a result of the shot peening process. It can be seen that, due to the damping effect, the analyzed frequency range corresponded to a slight variation of the thickness in which the signal was acquired. However, it can be distinguished that in more superficial layers there was a tendency to decrease, because the ferromagnetic phases present experienced a compressive residual stresses process that resulted in the mentioned decrease.

In addition, for smaller frequency ranges, carrying out the same comparative analysis, it can be observed that

Effect of Shot Peening Treatment on Residual Stress and Magnetic Barkhausen Noise of AISI 201LN and AISI 304L Stainless Steels

9

the transformation from austenite to martensite promoted the acquisition of signals with higher RMS$_{MBN}$ signals. Furthermore, this fact can be corroborated in the layers corresponding to the frequency range of 70 to 75 kHz, thus a strong sensitivity to the residual stresses state can be observed for this characterization technique in small depth variations.

Finally, as well as the measurements of hardness and residual stresses by X-ray diffraction, the treatment time of 30 seconds promoted the main changes in relation to the as-received condition, since there were no significant variations for the other conditions evaluated according to Figure 14.

4. Conclusions

In the present work, the microstructure changes as a result of the shot peening process in 201LN and 304L austenitic stainless steels and their effects on residual stresses behavior were investigated by X-ray diffraction technique, using sin$^2\psi$ method, and magnetic Barkhausen noise, and the following conclusions were:

1.   The shot peening process promoted austenitic transformation into ferromagnetic martensite with lower susceptibility in 304L steel, which also had a higher delta ferrite content in the initial condition compared to 201LN steel. The "fresh" martensite formed by this process initially produced a tensile residual stresses state, while the preliminary martensite plus delta ferrite became compressive.

2.   The major changes in hardness, ferromagnetic phases content, residual stresses and magnetic Barkhausen noise were detected in the first 30 seconds of shot peening time.

3.   The MBN was analyzed by two methods, spectral density frequency and band-pass filter, where the signal response was comparatively evaluated for the same frequency range near the resonance frequency of the sensor. The applied methods had similar behavior, with significant changes during the 30 seconds of the shot peening process.

4.   In both frequency analysis, changes mainly due to the stresses state of the ferromagnetic phases in layers of 0.1 mm were detected, showing that the MBN technique can become a powerful tool for characterizing residual stresses and microstructural changes caused by shot peening in austenitic stainless steels.

5. Acknowledgments

6. References

1.   Yang X, Liu M, Liu Z, Du C, Li X. Failure analysis of a 304 stainless steel heat exchanger in liquid sulfur recovery units. Eng Fail Anal. 2020;116:104729. http://dx.doi.org/10.1016/j.engfailanal.2020.104729.

2.   Nagaishi N, Okazaki S, Ogawa Y, Matsunaga H. Dynamic improvement of fatigue strength via local phase transformation in a circumferentially-notched austenitic stainless steel under fully-reversed loading condition. Scr Mater. 2020;176:126-30. http://dx.doi.org/10.1016/j.scriptamat.2019.09.014.

3.   Corradi M, Di Schino A, Borri A, Rufini R. A review of the use of stainless steel for masonry repair and reinforcement. Constr Build Mater. 2018;181:335-46. http://dx.doi.org/10.1016/j.conbuildmat.2018.06.034.

4.   Borgioli F, Galvanetto E, Bacci T. Corrosion behaviour of low temperature nitrided nickelfree, AISI 200 and AISI 300 series austenitic stainless steels in NaCl solution. Corros Sci. 2018;136:352-65. http://dx.doi.org/10.1016/j.corsci.2018.03.026.

5.   Pardal JM, Tavares SSM, Tavares MT, Garcia PSP, Velasco JAC, Abreu HFG, et al. Influence of carbon content on the martensitic transformation of titanium stabilized austenitic stainless steels. Int J Adv Manuf Technol. 2020;108:345-56. http://dx.doi.org/10.1007/s00170020-05138-8.

6.   Lu J, Hultman L, Holmström E, Antonnson KH, Grekl M, Li W, et al. Stacking fault energies in austenitic stainless steels. Acta Mater. 2016;111:39-46. http://dx.doi.org/10.1016/j.actamat.2016.03.042.

7.   Zheng C, Liu C, Ren M, Jiang H, Li L. Microstructure and mechanical behavior of an AISI 304 austenitic stainless steel prepared by cold-or cryogenic-rolling and annealing. Mater Sci Eng A. 2018;724:260-8. http://dx.doi.org/10.1016/j.msea.2018.03.105.

8.   Chen X, Zhou C, Zheng J, Zhang L. Effects of α′ martensite and deformation twin on hydrogen-assisted fatigue crack growth in cold/warm-rolled type 304 stainless steel. Int J Hydrogen Energy. 2018;43(6):3342-52. http://dx.doi.org/10.1016/j.ijhydene.2017.12.173.

9.   Kleber X, Barroso SP. Investigation of shot-peened austenitic stainless steel 304L by means of magnetic Barkhausen noise. Mater Sci Eng A. 2010;527:6046-52. http://dx.doi.org/10.1016/j.msea.2010.06.008.

10.   Bahadur A, Kumar BR, Chowdhury SG. Evaluation of changes in X-ray elastic constants and residual stress as a function of cold rolling of austenitic steels. Mater Sci Technol. 2004;20:387-92. http://dx.doi.org/10.1179/026708304225012170.

11.   Plaut RL, Herrera C, Escriba DM, Rios PR, Padilha AF. A short review on wrought austenitic stainless steels at high temperatures: processing, microstructure, properties and performance. Mater Res. 2007;10:453-60. http://dx.doi.org/10.1590/S1516-14392007000400021.

12.   Garcia-Martin J, González-Fernández R, Calleja-Saenz B, Ferreño-Blanco D. Measurement of hardness increase for shot-peened austenitic TX304HB stainless steel tubes with electromagnetic Non-Destructive testing. Measurement. 2020;149:106925. http://dx.doi.org/10.1016/j.measurement.2019.106925.

13.   Bahadur A, Mitra A, Kumar BR, Sagar SP. Evaluation and correlation of residual stress measurement in steel. J Nondestr Eval. 2007;26:47-55. http://dx.doi.org/10.1007/s10921-007-0019-8.

14.   Ding S, Tian GY, Dobmann G, Wang P. Analysis of domain wall dynamics based on skewness of magnetic Barkhausen noise for applied stress determination. J Magn Magn Mater. 2017;421:225-9. http://dx.doi.org/10.1016/j.jmmm.2016.08.030.

15.   ASTM: American Society for Testing and Materials. ASTM A240: Standard Specification for Chromium and Chromium-Nickel Stainless Steel Plate, Sheet, and Strip for Pressure Vessels and for General Applications. West Conshohocken, PA: ASTM International; 2020. http://dx.doi.org/10.1520/A0240_A0240M-20

16.   Curtze S, Kuokkala VT, Oikari A, Talonen J, Hänninen H. Thermodynamic modeling of the stacking fault energy of

austenitic steels. Acta Mater. 2011;59(3):1068-76. http://dx.doi.org/10.1016/j.actamat.2010.10.037.

17. Schneider H. Investment casting of high-hot strength 12% chrome steel. Foundry Trade J. 1960;108:562-3.

18. Bermejo MAV, DebRoy T, Hurtig K, Karlsson L, Svensson LE. Towards a map of solidification cracking risk in laser welding of austenitic stainless steels. Phys Procedia. 2015;78:230-9. http://dx.doi.org/10.1016/j.phpro.2015.11.033.

19. Rajasekhar K, Harendranath CS, Raman R, Kulkarni SD. Microstructural evolution during solidification of austenitic stainless steel weld metals: a color metallographic and electron microprobe analysis study. Mater Charact. 1997;38(2):53-65. http://dx.doi.org/10.1016/S1044-5803(97)80024-1.

20. Huang F, Wang X, Zhang J, Ji C, Fang Y, Yu Y. In situ observation of solidification process of AISI 304 austenitic stainless steel. J Iron Steel Res Int. 2008;15(6):78-82. http://dx.doi.org/10.1016/S1006-706X(08)60271-X.

21. ASTM: American Society for Testing and Materials. ASTM E112: Standard Test Methods for Determining Average Grain Size. West Conshohocken, PA: ASTM International; 2013. http://dx.doi.org/10.1520/E0112-13.

22. Degen T, Sadki M, Bron E, König U, Nénert G. The HighScore suite. Powder Diffr. 2014;29:S13-8. http://dx.doi.org/10.1017/S0885715614000840.

23. ASTM: American Society for Testing and Materials. ASTM A370: Standard Test Methods and Definitions for Mechanical Testing of Steel Products. West Conshohocken, PA: ASTM International; 2020. http://dx.doi.org/10.1520/A0370-20

24. Liu ZY, Fu CH, Sealy MP, Zhao Y, Guo YB. Benchmark Burnishing with Almen Strip for Surface Integrity. Procedia Manuf. 2017;10:456-66. http://dx.doi.org/10.1016/j.promfg.2017.07.027.

25. Talonen J, Hänninen H. Energetics of plastic deformation of metastable austenitic stainless steel. Steel Res Int. 2007;78:260-5. http://dx.doi.org/10.1002/srin.200705889.

26. ASTM: American Society for Testing and Materials. ASTM E18: Standard Test Methods for Rockwell Hardness of Metallic Materials. West Conshohocken, PA: ASTM International; 2020. http://dx.doi.org/10.1520/E0018-20

27. Stresstech. [Internet]. Stresstech Bulletin 2: The properties of Barkhausen noise. cited 2020 Sep 27]. Available from: http://www.stresstech.com/wp-content/uploads/2020/08/properties-of-barkhausen-noise.pdf

28. Tiitto S, Säynäjäkangas S. Spectral Damping in Barkhausen Noise. IEEE Trans Magn. 1975;11:1666-72. http://dx.doi.org/10.1109/TMAG.1975.1058960.

29. Capó-Sánchez J, Padovese L. Magnetic Barkhausen noise measurement by resonant coil method. J Magn Magn Mater. 2009;321(18):L57-L62. http://dx.doi.org/10.1016/j.jmmm.2009.03.070.

30. Zerovnik P, Grum J. Determination of residual stresses from the Barkhausen noise voltage signal. In: Grum J, editor. 10th International Conference of the Slovenian Society for Non-Destructive Testing 2009: Application of Contemporary Non-Destructive Testing in Engineering; 2009 Sep 1-3; Ljubljana, Slovenia. Slovenia: The Slovenian Society for Non-Destructive Testing; 2009. Vol. 1, p. 437-446.

31. Osoba LO, Elemuren RA, Ekpe IC. Influence of delta ferrite on corrosion susceptibility of AISI 304 austenitic stainless steel. Cogent Eng. 2016;3:1150546. http://dx.doi.org/10.1080/23311916.2016.1150546.

32. Ben Rhouma A, Amadou T, Sidhom H, Braham C. Correlation between microstructure and intergranular corrosion behavior of low delta-ferrite content AISI 316L aged in the range 550-570°C. J Alloys Compd. 2017;708:871-86. http://dx.doi.org/10.1016/j.jallcom.2017.02.273.

33. Abramoff MD, Magalhaes PJ, Ram SJ. Image processing with ImageJ. Biophoton Int. 2004;11(7):36-42.

34. Kana V, Pernica V, Zadera A, Kritis V. Comparison of methods for determining the ferrite content in duplex cast steels. Arch Foundry Eng. 2019;19:85-90. http://dx.doi.org/10.24425/afe.2019.127121.

35. Fitzpatrick ME, Fry AT, Holdway P, Kandil F, Shackleton J, Suominen L. Determination of Residual Stresses by X-ray Diffraction. Teddington: National Physical Laboratory; 2005.

36. Tandon V, Thombre MA, Patil AP, Taiwade RV, Vashishtha H. Effect of heat input on the microstructural, mechanical, and corrosion properties of dissimilar weldment of conventional austenitic stainless steel and lownickel stainless steel. Metall Microstruct Anal. 2020;9:668-77. http://dx.doi.org/10.1007/s13632-020-00681-y.

37. Talha M, Behera CK, Sinha OP. A review on nickel-free nitrogen containing austenitic stainless steels for biomedical applications. Mater Sci Eng C. 2013;33(7):3563-75. http://dx.doi.org/10.1016/j.msec.2013.06.002.

38. Peral LB, Quintero A, Vielma AT, Barbés MF, Fernández-Pariente I. TEM evaluation of steel nanocrystalline surfaces obtained by severe shot peening. Surf Coat Tech. 2021;418:127238. http://dx.doi.org/10.1016/j.surfcoat.2021.127238.

39. O'Sullivan D, Cotterell M, Meszaros I. The characterisation of work-hardened austenitic stainless steel by NDT micro-magnetic techniques. NDT Int. 2004;37(4):265-9. http://dx.doi.org/10.1016/j.ndteint.2003.10.001.

40. Matweb Material Property Data. [Internet]. AK Steel 201LN Austenitic Stainless steel cited 2020 Nov 11]. Available from: http://www.matweb.com/search/datasheet.aspx?matguid=4d2c7e6d770b44ccae68065dbce46530

41. Matweb Material Property Data [Internet]. AK Steel 304L Austenitic Stainless steel [cited 2020 Nov 11]. Available from: http://www.matweb.com/search/datasheet.aspx?matguid=8379d9f31c8243acbf350273660ea83e&ckck=1